HHS Public Access

Author manuscript

Cell. Author manuscript; available in PMC 2023 December 08.

Published in final edited form as:

Cell. 2022 December 08; 185(25): 4756–4769.e13. doi:10.1016/j.cell.2022.11.008.

Embryonic origins of adult pluripotent stem cells

Julian O. Kimura,

Marcela Bolaños-Rodriguez,

Lorenzo Ricci,

Mansi Srivastava[1,*]

Department of Organismic and Evolutionary Biology, Museum of Comparative Zoology, Harvard University, Cambridge, MA 02138

Summary

Although adult pluripotent stem cells (aPSCs) are found in many animal lineages, mechanisms for their formation during embryogenesis are unknown. Here, we leveraged *Hofstenia miamia*, a regenerative worm that possesses collectively pluripotent aPSCs called neoblasts, and produces manipulable embryos. Lineage-tracing and functional experiments revealed that one pair of blastomeres gives rise to cells that resemble neoblasts in distribution, behavior, and gene expression. aPSCs include transcriptionally-distinct subpopulations expressing markers associated with differentiated tissues; our data suggest that despite their heterogeneity, aPSCs are derived from one lineage, not from multiple tissue-specific lineages during development. Next, we combined single-cell transcriptome profiling across development with neoblast cell lineage tracing and identified a molecular trajectory for neoblast formation that included transcription factors Hes, FoxO, and Tbx. This identification of a cellular mechanism and molecular trajectory for aPSC formation opens the door for *in vivo* studies of aPSC regulation and evolution.

Graphical Abstract

[*]Correspondence: mansi@oeb.harvard.edu.

[1]Lead Contact

Author Contributions

J.O.K. was involved in the conceptualization, investigation, analysis, and writing of the project. M. B-R. performed functional studies, contributing to investigation, analysis, and writing of the project. L.R. generated the transgenic line utilized in this project and contributed to writing. M.S. was responsible for funding acquisition, conceptualization, analysis, and writing of the project.

Declaration of Interests

The authors declare that they do not have any competing interests.

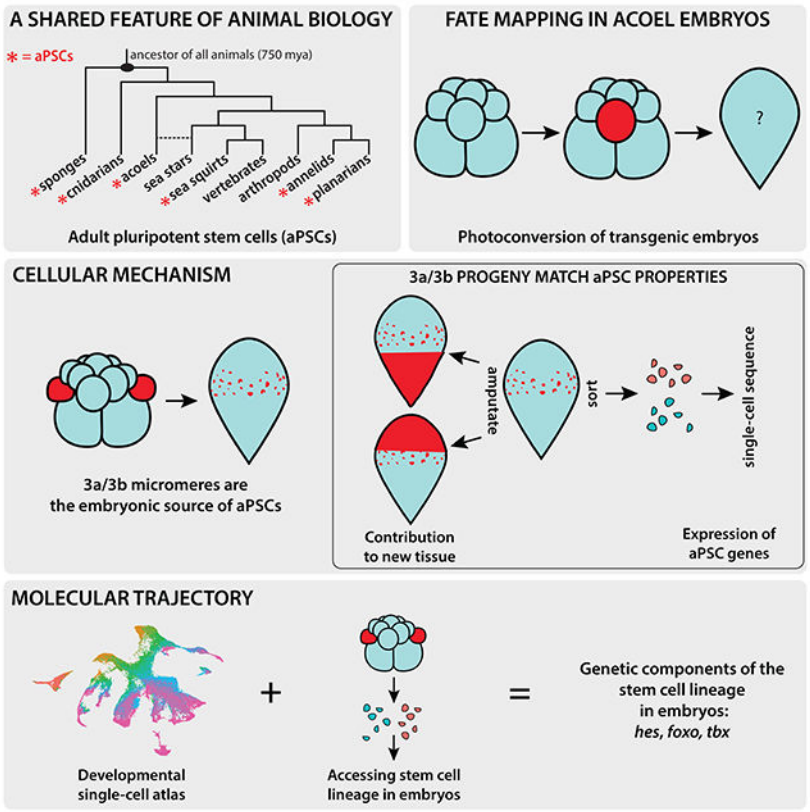

In Brief

Lineage-tracing and functional experiments in the regenerative worm *Hofstenia miamia* reveal that a single pair of blastomeres gives rise to cells that resemble neoblasts in distribution, behavior, and gene expression.

Introduction

Populations of adult pluripotent stem cells (aPSCs) are found in many distantly-related invertebrate animals, where they facilitate whole-body regeneration and/or homeostatic tissue turnover[1] (Fig. 1A). Some examples include the neoblasts of planarians[2–4], the *i*-cells of some cnidarians[5,6], and the archaeocytes of sponges[7,8]. In the majority of these systems, aPSCs express shared markers, including orthologs of Piwi and other proteins associated with germ cells[9]. Given these shared molecular properties across 750 million years of animal evolution, aPSCs are possibly a fundamental feature of animal biology that is notably absent in mammals. Although the mechanisms underlying the regulation of pluripotency in mammalian embryonic stem cells (ESCs) are known[10], these cells lose their potency over the course of embryonic development and aPSCs are absent in the adult body plan. Therefore, studies in animals with aPSCs are needed to uncover how pluripotent stem cells are first specified and then maintained until adulthood *in vivo*. The timing of emergence of functional stem cells (in planarians)[11] and the expression of aPSC marker genes (in cnidarians)[12,13] have been investigated, but the underlying cellular and molecular

mechanisms for the formation of aPSCs remain unknown. Here, we sought to determine the cellular source of aPSCs and to identify molecular regulators that could be involved in aPSC formation during embryogenesis.

The highly regenerative acoel *Hofstenia miamia* possesses a population of collectively pluripotent stem cells, *i.e.* aPSCs, referred to as 'neoblasts'[14,15]. The embryos of *Hofstenia* undergo a stereotyped cleavage program (Fig. 1B), enabling an investigation of the cellular source of aPSCs[14,15]. *Hofstenia* neoblasts express Piwi orthologs, are required for regeneration[14], and enable homeostatic tissue turnover[16]. These cells are present in the worms upon hatching (Fig. S1A) and therefore must be made during embryogenesis. Single-cell transcriptome profiling suggests that the neoblast population of adult *Hofstenia* is composed of transcriptionally distinct subsets of cells that express markers associated with differentiated tissues[16]. Planarian neoblasts[17–19] and cnidarian *i*-cells[6] are also known to be transcriptionally heterogeneous. In view of this heterogeneity, two cellular mechanisms could explain the formation of neoblasts in *Hofstenia*: 1) they are derived from one embryonic lineage and become heterogeneous as they begin to differentiate, 2) they are derived from multiple, tissue-specific embryonic lineages – cell populations first acquire tissue type identity, and within these tissue-specific lineages, corresponding neoblast subtypes are specified. The latter scenario would bear similarity to stem cells in vertebrates, where tissue-associated stem cells originate in specific lineages, *e.g.* mesodermal progenitors give rise to muscle and muscle satellite cells and endodermal progenitors give rise to intestinal epithelia and intestinal stem cells.

To assess these mechanistic scenarios, we labeled and traced the blastomeres of *Hofstenia* embryos through development to hatching, and identified one pair of cells at the 16-cell stage as the major embryonic source of neoblasts. We then combined our ability to trace and isolate the neoblast lineage with a single-cell atlas of embryos and identified a molecular trajectory associated with the formation of neoblasts.

Results

Lineage tracing in transgenic embryos reveals the fate map of Hofstenia blastomeres

We utilized transgenic embryos with constitutive presence of Kaede protein, which can be photoconverted in individual cells (blastomeres) to trace each cell's contribution to tissues in hatched worms, with the ultimate goal of determining the cellular sources of neoblasts (Fig. 1C–E, Fig. S1B), see generation and maintenance of transgenic lines section in Method Details). We found that the photoconverted labeling was stable, and persisted beyond the completion of embryogenesis (Fig. 1F). *Hofstenia* embryos display a stereotyped cleavage program with clear correspondence of blastomeres across embryos[15] (Fig. 1B), which enabled us to systematically photoconvert each blastomere in 8-cell stage embryos and generate a complete fate map by correlating the distribution and morphology of labeled progeny to those of known tissue markers (Fig. 1E–G, S1A, S1C, and S1D). Overall, the highly reproducible and distinct labeling of tissues in these experiments highlighted that the photoconverted Kaede protein had high perdurance and was not leaky, making it an effective tool for lineage tracing.

Photoconversion of embryonic cells followed by time-lapse imaging and visualization of converted progeny in hatched worms identified the embryonic sources of major cell types (Fig. 1E–G, S1C–D, Videos S1–S3). Briefly, early cleavage in *Hofstenia* proceeds as follows: The first cleavage results in the 2-cell stage consisting of equal-sized cells (A and B). Next, these two cells divide asymmetrically, giving rise to the 4-cell stage with two small cells at the animal pole (1a and 1b) called micromeres, and two large cells at the vegetal pole (1A and 1B) called macromeres. The prefix "1" in the names of these cells reflects that they are the products of the first asymmetric cleavage of the A and B cells. The 1a and 1b micromeres divide, producing cells named $1a^1/1a^2$ and $1b^1/1b^2$ respectively, resulting in the 6-cell stage embryo. Finally, the 1A and 1B macromeres cleave asymmetrically to produce two corresponding daughter cells each (now prefixed with "2", to reflect that they are produced by the second asymmetric cleavage): micromeres 2a and 2b, and macromeres 2A and 2B to reach the 8-cell stage[15] (Fig. 1B). A previous embryonic fate-map study of another acoel had revealed that distinct cell fates were associated with blastomeres at the 8-cell stage[27], and therefore, we focused our efforts on understanding the fates of blastomeres in 8-cell stage *Hofstenia* embryos.

Lineage tracing by photoconversion revealed that the animal-most progeny of 1a/1b micromeres, $1a^1/1b^1$, produced the nervous system whereas the vegetal progeny, $1a^2/1b^2$, gave rise to muscle, epidermis, and pharyngeal tissue (Fig. 1F–G). The second set of micromeres, 2a/2b, gave rise to muscle and the antero-lateral epidermis. The macromeres, 2A/2B, gave rise to multiple distinct tissues including the statocyst, gut, and a population of internal cells in the midsection of the animal along the anterior-posterior axis (Fig. 1F–G). Overall, these data showed that the fates of blastomeres are restricted by the 8-cell stage, and that some tissues such as the nervous system are derived from one source ($1a^1/1b^1$) whereas others such as muscle and epidermis are derived from multiple sources ($1a^2/1b^2$, 2a/2b).

We followed these blastomeres at the 8-cell stage during development to characterize the timing and modes by which these blastomere progenies internalized. $1a^1/1b^1$ progeny labeled a patch of external cells during the Gastrula stage, but were internalized through delamination at a site adjacent to the "dimple" during the Dimple stage (Fig. S1C and Video S1). The progeny of the $1a^2/1b^2$ pair exhibited a pattern in which half of the progeny internalized at the Dimple stage, whereas the other half remained on the exterior of the embryo until hatching (Fig. S1C). Single photoconversion experiments provided greater resolution into these distinct behaviors – the majority of $1a^2$ progeny internalized at the Dimple stage through apical constriction (Video S2), while the progeny of $1b^2$ largely remained on the exterior of the embryo until hatching (Video S3). The 2a/2b progeny labeled bilaterally symmetric patches of cells on the left and right side of the embryo throughout development (likely corresponding to future epidermis), and only a small proportion of them were seen to become internalized at the Dimple stage (likely corresponding to future muscle) (Fig. S1C). The majority of 2A/2B progeny were internalized at the Gastrula stage, with the exception of two bilaterally symmetric patches of cells that were internalized via delamination at the Dimple stage (Fig. S1C and Video S4).

These experiments also allowed us to correlate the broad spatial maps of blastomeres and their progeny in hatched worms (Fig. 1F–G, Figs. S1D–S1H, Videos S1–S4). The progeny

of most blastomere pairs (derived from the two cells, A and B, made upon first cleavage), showed symmetry along the left-right axis and their fates can be summarized using data from embryos where both cells of a pair are converted (Figs. 1E–F show conversions of paired cells, Fig. S1D shows single blastomere conversions). Macromeres 2A/2B showed slight differences in left-right symmetry in that both produced gut and midsection cells, but only one, which we designate here as 2B, produced the statocyst. More notably, the $1a^2$ and $1b^2$ pair deviated more drastically from this pattern of left-right symmetry. The majority of the $1a^2$ progeny became internalized at the “dimple”, whereas the small proportion of the progeny that remained at the surface invaginated later during development to form the pharynx, an anterior structure (Fig. S1D, S1E, Video S2). The majority of $1b^2$ progeny remained on the external periphery of the embryo, and ultimately gave rise to the majority of the epidermis that covered the anterior, posterior, dorsal, and ventral midlines of the animal (Fig. S1D, Video S3). $1b^2$ progeny also gave rise to muscle, likely from a small proportion of cells that internalized at the Dimple stage (Fig. S1D). Given this distribution of progeny, we inferred that the position of $1a^2$ at the 8-cell stage corresponds to the anterior of hatched worms, and $1b^2$ corresponds to the posterior. Furthermore, we correlated the relationship of the animal pole of the embryos to the future adult axis by photoconverting the surface of the embryo at the site where $1a^1/1b^1$ progeny were internalized. This resulted in the labeling of the dorsal epidermis in the hatched worms, suggesting that the animal-vegetal axis of the early embryo corresponds to the dorsal-ventral axis respectively (Fig. S1F). Therefore, in addition to showing the origins of major cell types, our fate map of the 8-cell embryo revealed the correspondence of embryonic and adult axes (Fig. S1G).

Progeny of the 3a/3b blastomeres resemble neoblasts

Among the various blastomere fates observed, the midsection cells derived from the 2A and 2B blastomeres were of interest as their parenchymal, midsection distribution was reminiscent of that of neoblasts (Fig. 1F–G and S1A). Given that the 2A and 2B macromeres also gave rise to the statocyst and gut, we sought further resolution on the origins of these distinct cell populations. We waited for these two blastomeres to cleave once more, and traced the fates of their daughter cells at the 16-cell stage. 2A and 2B cleave asymmetrically to generate micromeres, 3a and 3b, and macromeres, 3A and 3B (Fig. 2A). The change in nomenclature of the blastomeres, *i.e.* the prefix ‘2’ being replaced with the prefix ‘3’, indicates that 3a/3b and 3A/3B are the product of the third asymmetric cleavage of the macromere lineage. Overall, we found that the distinct cell populations observed in hatchlings derived from labeled 2A/2B blastomeres (statocyst, gut, midsection cells) were made by different daughter cells produced by 2A/2B.

The progeny of 3A/3B macromeres became internalized at the Gastrula stage and gave rise to the gut and statocyst (Fig. 2B–D). The lack of muscle progeny from the only cells that generate endodermal progeny (3A/3B) suggests a possible lack of an endomesodermal precursor in *Hofstenia*, similar to observations in annelids[20–22]. The progeny of 3a/3b micromeres formed two patches on the exterior at the Gastrula stage that became internalized at the Dimple stage, and gave rise to the internal, midsection cells we had observed in the 2A/2B lineage-trace (Fig. 1F–G, 2B–D). These results gave us increased resolution for the origins of hatchling tissues derived from 2A/2B – the macromere

daughters of 2A/2B, 3A/3B, made the gut and statocyst and the micromere daughters of 2A/2B, 3a/3b, made midsection cells. The lineage traces of the daughter cells (3a/3b and 3A/3B) together added up to the fate map of the mother cells (2A/2B), further corroborating our fate-mapping approach.

Importantly, for our objective of identifying the embryonic origins of neoblasts, the increased resolution from tracing the fates of 3a/3b and 3A/3B gave a cleaner label of the midsection population. In hatchlings derived from 3a/3b-labeled embryos, closer inspection of the midsection cells revealed that they possessed large, cytoplasmic extensions, and confirmed their internal, midsection distribution reminiscent of neoblasts (Fig. 2C, S1A, and S2). Single conversions of the 3a/3b cells showed that they both gave rise to these midsection cells, and showed left-right symmetry (Fig. S2). Thus, we next sought to test if the progeny of 3a/3b micromeres exhibited functional characteristics of neoblasts by assaying them together.

Progeny of the 3a/3b blastomeres exhibit functional characteristics of neoblasts

Hofstenia neoblasts exhibit three key functional properties: 1) contribution to newly regenerated tissue, 2) contribution to homeostatic turnover of mature tissue in the animal[16], and 3) radiation sensitivity[14]. We sought to assess whether the progeny of 3a/3b also displayed these characteristics in hatched worms.

To test whether the 3a/3b progeny cells contributed to newly regenerated tissue, we photoconverted 3a/3b, amputated the worms upon hatching, and focused on the outgrowth of new tissue at the wound site, the blastema (Fig. 3A). If 3a/3b progeny cells can contribute to new tissue, we would expect the blastema to possess red, photoconverted cells. As a control, we converted the $1a^1/1b^1$ micromeres that gave rise to neurons, which in theory should not contribute to regenerated tissue, and should not result in red labeling in the blastema. Strikingly, we detected substantial numbers of red, photoconverted cells in the blastema among the animals derived from 3a/3b-labeled embryos. In the $1a^1/1b^1$-labeled animals, only a few red neurons, likely ones that were already present at the wound site, were present in the blastema during both head and tail regeneration (Fig. 3A). Additionally, we assessed the ability of the progeny of all other blastomeres at the 16-cell stage to populate the blastema and did not detect substantial contributions (Fig. S3A, S3B, and S3C), which suggests that the progeny of 3a/3b are the major source of cells in the blastema during regeneration.

Given that neoblasts are the only somatic proliferative cells in *Hofstenia*, we expect them to contribute to continuous homeostatic turnover of tissues in the adult worm and to be sensitive to radiation[14]. To study homeostasis, we converted the 3a/3b blastomeres and imaged the worms one week after hatching (Fig. 3B). Compared to newly hatched worms, those imaged a week after hatching exhibited red labeling in epidermal and muscle cells. We also found that the midsection cell population, the putative neoblasts, had expanded in number in comparison to newly hatched, labeled worms (Fig. 3B). We did not, however, detect red labeling in neurons, pharynx, or the gut. This could be because the homeostatic turnover rates for these tissues are low during the first week upon hatching. Alternatively, it could be that there are other, minor sources of neoblasts that are contributing to these tissue

types. It is also possible that the label is diluted because of the number of mitoses needed to make these tissues– or, in the case of the gut, because photoconverted protein would spread through a large syncytial tissue[23]. Meanwhile, the labeling of other blastomeres did not result in the expansion of red color to other differentiated tissue types (*e.g.*, $1a^1/1b^1$ progeny, which label neurons in hatched worms, did not contribute to labeled muscle or epidermis.) (Fig. S3D). This is consistent with the interpretation that other cell populations, derived from blastomeres other than 3a/3b, do not exhibit neoblast-like properties. Additionally, we found that the 3a/3b progeny cells, but not the progeny of other blastomeres, were completely ablated within seven days upon exposure to radiation (Fig. 3C and S3E).

We found that these functional characteristics of neoblasts are likely acquired by 3a/3b progeny late in development. *piwi-1* was expressed among all embryonic cells until just before hatching at the Pigmented Prehatchling stage, when the expression of *piwi-1* became regionally restricted to resemble a neoblast-like distribution. (Fig. S3F). Double-labeling of *Hofstenia* embryos with *piwi-1* and the mitotic marker H3P showed that mitotic cells were always associated with *piwi-1*$^+$ cells across development. Mitotic cells did not show regional restriction until the Pigmented Prehatchling stage, the same timepoint when we detected *piwi-1* expression in a pattern reminescent of neoblasts (Fig. S3F). This suggested that neoblasts acquire the property of being the only proliferative somatic cells in *Hofstenia* right before hatching. Consistent with this finding, Pigmented Prehatchling stage embryos were able to regenerate both anterior and posterior structures upon amputation (Fig. S3G). These data suggest that although neoblasts are fated as early as the 16-cell stage, in 3a/3b micromeres, they likely do not acquire adult neoblast function until late in development, similar to planarian neoblasts[11].

Given that the functional testing of 3a/3b progeny supported our hypothesis that 3a/3b are the likely source of neoblasts, we next asked if 3a/3b blastomeres are required for the formation of aPSCs in *Hofstenia*. Laser-ablation of 3a/3b blastomeres resulted in hatchlings where *piwi-1* was still detected in its typical expression pattern (Fig. S3H). This could be due to regulative development, where other embryonic sources can compensate for the loss of the normal source of a tissue. To test for regulative capacities of other tissues in *Hofstenia*, we also ablated the $1a^1/1b^1$ blastomeres, which give rise to the nervous system. *In situ* hybridization studies of the neural marker *gad-1* showed a normal expression pattern in hatchlings derived from $1a^1/1b^1$-ablated embryos (Fig. S3H). Altogether this suggests that *Hofstenia* embryos may be capable of regulative development where they are able to compensate for the loss of cells that would normally produce specific tissues. Regardless, although embryos can compensate for the loss of 3a/3b, our experiments consistently point to 3a/3b as the source of neoblast-like cells in *Hofstenia*.

Progeny of the 3a/3b blastomeres exhibit molecular properties of neoblasts

As an independent assessment of neoblast chatacteristics, we next sought to ask if 3a/3b progeny displayed molecular properties associated with neoblasts at the time of hatching. To determine the transcriptomic profile of 3a/3b progeny cells, we photoconverted 3a/3b, and applied fluorescence-activated cell sorting (FACS) to separate the cells based on converted (red) vs. unconverted (green) fluorescence. To obtain sufficient material for this experiment,

we pooled hatched worms derived from 18 photoconverted embryos. Stage-matched early embryos in *Hofstenia* do not hatch perfectly synchronously, which meant 3a/3b progeny in some of the worms could include cells undergoing differentiation for postembryonic growth. This would impact their levels of red fluorescence as well as their transcriptional profiles. In view of this expected heterogeneity, we performed single-cell RNA-sequencing and sought to understand transcriptional diversity among red (3a/3b progeny) and green cells (progeny of other blastomeres) (Fig. 4A, Fig. S4A). Roughly half of the red cells expressed the neoblast marker *piwi-1* highly, whereas the majority of green cells did not (p-value = 7.767e-10, Wilcoxon Ranked Sum Test) (Fig. 4B).

Next, we performed unsupervised clustering on a pooled dataset of red and green cells, and assigned identities to these clusters by assessing the expression of known marker genes for cell types determined in the *Hofstenia* single-cell atlas[16] (Fig. S4B, Table S1). We identified seven cell clusters that likely represent epidermal, neural, digestive, endodermal progenitor, endoderm-like II, endoderm-like I, neoblasts (Fig. 4C), and an eighth cell cluster that we found to be present in a previously published single cell RNAseq dataset based on common marker gene expression[16]. We determined this eighth cluster is likely a secretory cell type based on marker gene expression and GO analysis which included terms such as vesicle mediated transport and protein glycosylation (Fig. 4C, S4C, and Table S1). The neoblast cluster consisted almost entirely of red, photoconverted cells (52/54 cells), suggesting that the majority of isolated cells that exhibited a neoblast-like transcriptomic profile were 3a/3b progeny (Fig. 4D). This was further highlighted when the proportion of cell types were visualized in a pie chart, showing a stark difference in the numbers of red vs. green cells placed in the neoblast cluster (Fig. 4D).

Although imaging of hatchlings derived from 3a/3b-converted embryos did not show clear labeling of other, non-neoblast cells, we found red cells within other cell type clusters in our single-cell analysis (Fig. 4C and 4D). These cells could result from 1) differentiation of 3a/3b-derived neoblasts, or 2) direct contribution of 3a/3b to differentiated tissue. The presence of red cells in the endodermal progenitor cluster, which represents putatively lineage-primed progenitors[16], suggests that tissues are undergoing postembryonic differentiation at or soon after hatching. The larger proportion of red cells in the epidermal cluster relative to other differentiated cell clusters could reflect differences in rates of differentiation of tissues, *e.g.* neoblasts may be contributing to epidermis more than to other tissues upon hatching. Overall, these data suggest that 3a/3b can contribute to differentiated tissues, directly or indirectly (through neoblasts) upon hatching, and further experimentation is needed to distinguish between the relative contributions of these two mechanisms. Here, we were focused on whether bona fide neoblasts are derived from 3a/3b or from other blastomeres, and our analysis strongly indicated that the vast majority of cells that match the transcriptional profile of neoblasts were indeed derived from 3a/3b (Fig. 4D).

We next sought to rigorously assess the significance of the different proportions of cell types found within the red and green cells. A chi-squared test of independence showed that the composition of cell types in the red and green cells is statistically significantly different (p = 3.375e-16) (Fig. 4D). We then determined the degree of association of each cell type to either the red vs. green cells by generating a contingency table of Pearson residuals (Fig.

4E). We found that the number of cells in the neoblast cluster was a key defining factor of both red and green cells, with red cells having a positive correlation with neoblasts and green cells having a negative correlation with neoblasts. Furthermore, the red cells were negatively correlated with the majority of other cell types detected, whereas green cells were positively correlated. Altogether, this suggests that the red cells are largely defined by the presence of neoblasts (as defined based on transcriptome profiles), while the green cells are defined by their absence (Fig. 4E). This evidence suggests that 3a/3b blastomeres are a major source of neoblasts in *Hofstenia*.

Embryonic single-cell atlas and cell lineage tracing identify a molecular trajectory for neoblast formation

While the acquisition of neoblast functional characteristics occurs late in development (Fig. S3F and S3G), the knowledge that 3a/3b micromeres are fated to produce neoblasts can be leveraged to study the ontogeny of neoblasts. Therefore, we next sought to identify molecular components that are associated with the formation of aPSCs in *Hofstenia* embryos.

We reasoned that by profiling transcription at the single-cell level over developmental time, we could identify cells whose transcriptional states implicate them as part of the neoblast lineage and ask which molecular players drive their progression towards a bona fide neoblast identity. To generate an embryonic single-cell atlas, we used the droplet-based platform, InDrops[24], to obtain the transcriptomes of ~51,000 cells spanning 8 different timepoints of development from 30 hours post laying (hpl) to just before hatching (145 hpl) (Fig. 5A). Uniform Manifold Approximation and Projection (UMAP) analysis of a merged dataset of these embryonic cells and of cells from hatched worms[16,25] recovered a graph with a branching pattern (Fig. 5B). Each branch was populated with cells from different stages in correct chronological order, with cells from hatched worms lying at the tips of the branches. Projection of known differentiated cell markers present in the hatchling dataset showed that each of the branch tips corresponded to a differentiated cell type, suggesting that our dataset likely captured cells undergoing differentiation towards these cell fates (Fig. 5B and Fig S5A).

To explicitly identify putative differentiation paths and the molecular components underlying them, we applied the trajectory inference tool URD[26] and obtained a tree with the Gastrula stage (30 hpl) cells at its root and hatchling cell clusters placed at its tips (Fig. 5B). The branching order in this tree showed the timing of the divergence of molecular trajectories during development for cell types in hatched worms: the epidermal clade diverged first, at the Dimple stage (50 hpl); next, the endodermal trajectory diverged at the Post Dimple stage (65 hpl); muscle, neural, and neoblast branches formed a polytomy at the Pill stage (95 hpl). Surprisingly, the URD topology showed that trajectories for various tissue types diverge transcriptionally at a much later time relative to our fate map, which showed cells had become fated to become neuron, muscle, epidermis, and gut as early as the 8-cell stage. This could either mean that transcriptional differences between embryonic lineages do not become pronounced enough to be detected through single cell RNA-seq until the Gastrula stage, or active differentiation of tissues through transcriptional

changes does not occur until then. To determine whether our trajectory analysis captured the transcriptional dynamics of *Hofstenia* embryos effectively, we next applied differential expression analysis to the terminal branches. This yielded putative marker genes for the corresponding cell types (Table S2). *in situ* hybridization studies of these marker genes corroborated both the timing of developmental expression and tissue identities of the cells placed along these branches (Fig. S5B and S5C). For example, the gut lineage marker *s61a2* was found to be expressed starting at the Post Dimple stage (80 hpl) in an internal region of the embryo. This internal expression pattern persisted until the Hatchling Juvenile stage, where it matched the expected distribution of digestive cells (Fig. S5C and S1A). Overall, these data suggested that the trajectory tree constructed by URD does indeed reflect transcriptional changes in the embryonic cells of *Hofstenia*. Interestingly, the well-studied marker of neoblasts in hatched worms, *piwi-1*, was expressed broadly in cells across stages of development, corroborating in expression studies via *in situ* hybridization in embryos (Fig. S3F, S5A). Our dataset did identify markers that labeled the neoblast trajectory in embryos more specifically, one of which, *neo*, specifically labeled neoblasts in hatchlings (Fig. S5A, S5B, S5C, and Table S2).

We next probed the URD branching topology to identify genes enriched in cells placed at the internodes leading to the neoblast branch (Table S2). These genes would represent putative regulators of neoblast formation. Among the handful of transcription factors found to be significantly highly expressed at internodes, *hes* emerged as also enriched in the terminal branch leading to neoblasts in hatched worms (Fig. 5C, Table S2). We found *hes* to be expressed in cells in the interior of embryos starting at the Post Dimple stage (80hpl), corroborating the timing of expression observed in the URD topology (Fig. 5D). These *hes*-expressing cells were distributed in a polarized manner in embryos and in hatchlings, where they matched the expression pattern of neoblast marker genes and were co-expressed *piwi-1* (Fig. S5D). These data suggest that *hes* could be expressed in embryonic cells that give rise to neoblasts in hatched worms.

Given that the URD topology infers molecular trajectories and not cellular lineages, the enrichment of *hes* in deep internodes leading to the neoblast branch could be the result of: 1) *hes* being expressed in embryonic progenitors for endodermal, muscle, and neuronal tissues in addition to progenitors for neoblasts, 2) *hes* being expressed only in progenitors for other tissues but not in neoblast progenitors. To distinguish between these possibilities, we isolated neoblast progenitors via FACS from Post Dimple stage (80hpl) embryos where 3a/3b had been photoconverted at the 8-cell stage (Fig. 5E and S5E). Unsupervised clustering of the transcriptomes of converted (red, neoblasts progenitors) and unconverted (green, other embryonic progenitors) cells yielded clusters that were composed of both red and green cells. These included clusters enriched for muscle and epidermal markers, as well as one that did not have any genes with enriched expression, referred to as “unknown” (Fig. 5F and S5F). More strikingly, the data identified two cell clusters – one predominantly populated with red cells, and the other with green cells – that yielded clearly enriched, specific marker genes. Cells in both clusters showed expression of *hes* (Fig. 5F, 5G, and S5F), corroborating the URD trajectory-based hypothesis that *hes* is present in progenitors for both neoblasts (red cells; 3a/3b progeny) and other tissues (green cells; progeny of other blastomeres).

Differential expression analysis across these clusters additionally revealed genes that were specifically enriched in a subset of neoblast progenitor cells (red cells), including two transcription factors, *foxo* and *tbx* (Fig. 5F, 5G, and Table S2). This suggested that *hes* may be a marker for progenitor-like states in general during development, but *foxo* and *tbx* would be specific to the neoblast lineage. *foxo* and *tbx* were co-expressed among 3a/3b progeny at the Post Dimple stage (80 hpl), consistent with having functions in the same lineage of cells (Fig S5G). To further bolster the hypothesis that *foxo* and *tbx* are associated with the neoblast lineage in embryos, we performed *in situ* hybridization studies which showed that both *foxo* and *tbx* were expressed in cells that also express *hes* during embryogenesis (Fig. 5H and S5H). Additionally, association of *foxo* and *tbx* with neoblasts was supported by observations in hatchlings: 1) *foxo*- and *tbx*-expressing cells were distributed in a neoblast-like pattern in hatchlings (Fig. S5I), 2) Double *in situ* hybridization of foxo and *tbx* with *piwi-1* in hatchlings showed co-localization, corroborating that both these transcription factors are expressed in neoblasts (Fig. 5I), 3) *foxo* and *tbx* RNAi resulted in reduced regeneration and *foxo* RNAi animals showed diminished *piwi-1* expression during homeostasis (Fig. S5J, S5K, and S5L), 4) *foxo* and *tbx* were enriched in the neoblast cluster of 3a/3b progeny in hatched worms (Fig. S5M). Altogether, the data show that *hes*, *foxo*, and *tbx* are part of the molecular trajectory for neoblast formation and point to the possibility that *foxo* and *tbx* may be specific regulators of neoblast formation during embryonic development.

Discussion

Here we generated a complete fate map of cells in early stage embryos of the highly regenerative acoel worm *Hofstenia miamia*, which showed important aspects of *Hofstenia* embryogenesis including the correspondence of embryonic and adult body axes and the lack of a common endomesodermal progenitor. Overall, the fates of *Hofstenia* blastomeres differ in many aspects from the fate map for another acoel [27], including the notable lack of an endomesodermal progenitor, a departure from the classical definition of gastrulation[20,21]. However, the possible lack of a common endomesodermal progenitor is not without precedent and has been reported in an annelid[22]. Most strikingly, our study revealed a cellular source of neoblasts, the aPSCs of acoels. Furthermore, we identified a molecular trajectory associated with the formation of these aPSCs.

A cellular mechanism for neoblast formation

The formation of neoblasts could have occurred through two different mechanisms. In one scenario, multiple embryonic cell lineages could contribute to the neoblast population in adults (Fig. 6A). In this case, tissue-associated neoblast subtypes could be derived from the distinct embryonic sources of their corresponding differentiated tissues. In the alternative scenario, the neoblast lineage could arise from a singular source and acquire heterogeneous, tissue-associated transcriptional profiles over time (Fig. 6A). We found that cells with neoblast characteristics arise from a specific set of early embryonic blastomeres called 3a and 3b, albeit they acquire these properties late in development. Altogether, the lack of detectable contribution to regeneration and homeostatic turnover, insensitivity to lethal doses of irradiation, and extremely low proportion of neoblast-like cells detected among

the progeny of all other blastomeres suggests that the 3a/3b blastomeres are the major source of neoblasts during *Hofstenia* embryogenesis. Thus, our data support the hypothesis that neoblasts likely form from a singular source early during development. Future studies of neoblast dynamics in adult worms will reveal whether the heterogeneous subsets of neoblasts formed in this manner are transcriptionally plastic and interconvertible in adult *Hofstenia*, as recently demonstrated in planarians[28].

The origin of aPSCs from a specific set of early embryonic cells is reminiscent of how the germline originates in some species[29]. In one species of annelid worm, the same early embryonic cell gives rise to the germline and to a putative stem cell population[30]– although the full potentials of these stem cells remain to be explored. In *Hofstenia*, neoblasts are expected to ultimately form the germline as animals reach sexual maturity[16], which suggests that 3a/3b could be a source both for aPSCs and the germline.

A molecular trajectory for neoblast formation

Our finding that one pair of cells serves as the major source of aPSCs in *Hofstenia* enabled us to obtain a molecular trajectory specifically associated with neoblast formation (Fig. 6B). Large-scale single-cell transcriptome sequencing can be used to infer molecular trajectories, which serve as a hypothesis for molecular processes that may underlie cellular lineages in development. We generated these hypotheses using an embryonic single-cell atlas for *Hofstenia*, and then we labeled (by photoconversion of 3a/3b) and isolated the embryonic precursors of neoblasts to directly assess the presence of hypothesized molecular components. The three transcription factors we identified in the neoblasts molecular trajectory all have known roles in regulating pluripotency and differentiation in other species. Homologs of Hes, which appears to be expressed in precursors of neoblasts and other tissues, are known to regulate differentiation of mouse embryonic stem cells (ESCs), where oscillations in the levels of Hes expression result in differential fates of stem cells[31]. FoxO and Tbx proteins, which appear to be specific to neoblast precursors in *Hofstenia*, are required for pluripotency in human and mouse ESCs respectively[32,33]. FoxO proteins are also known to be necessary for continuous self-renewal of hydra *i*-cells[34]. Future investigations of the mechanisms of action of these transcription factors in *Hofstenia* embryos will reveal if the roles they play in neoblast biology are similar to those observed in other systems.

Future directions

Our study reveals the embryonic cellular source of adult pluripotent stem cells, which are present in many lineages across the animal tree of life and therefore are an important feature of animal biology. The identification of an embryonic neoblast lineage and its molecular components serves as an entry point to dissect genetic mechanisms for the formation and maintenance of aPSCs during embryonic development. In addition to deciphering the key regulators of stem cells, these mechanisms will also enable a robust assessment of the putative homology of aPCSs in distantly-related species.

Limitations of the Study

The lineage tracing performed in this study relies on a photoconverted protein, which showed high stability in over the time courses followed, but this is approach is sensitive to differential rates of cleavage across embryonic cell lineages. For example, it is possible that the signal would be too dilute in daughter lineages that underwent high rates of cell proliferation, limiting the ability to detect complete detection of all blastomere progeny. The plate-based sequence analyses alleviate these concerns to some extent, as large discrepancies between photoconversion-based fate-mapping would be detectable via those data.

STAR Methods Text

RESOURCE AVAILABILITY

Lead contact—Further information and requests for resources and reagents should be directed to and will be fulfilled by the lead contact, Mansi Srivastava (mansi@oeb.harvard.edu).

Materials availability—All unique/stable reagents generated in this study are available from the lead contact with a completed materials transfer agreement. Plasmids with transgene constructs generated in this study are available from Addgene and the accession number is provided in the key resources table.

Data and code availability

- Single-cell RNA-seq data have been deposited at SRA under Bioproject Accession numbers: PRJNA889328, PRJNA887118, and PRJNA888438 for the FACS sorted 3a/3b progeny dataset at hatching, FACS sorted 3a/3b progeny dataset at 80 hours post laying, and the embryonic and postembryonic datasets respectively. Gene sequences in this study are deposited to GenBank. They are publicly available as of the date of publication. Accession numbers for the gene sequences in Genbank are listed in the key resources table. Microscopy data reported in this paper will be shared by the lead contact upon request.
- All original code has been deposited at Github (https://github.com/JulianKimura/Kimura_2022_Rscripts for single cell RNAseq analyses in R, and https://github.com/JulianKimura/SMARTseq_Pipeline for generating SMARTseq matrices) and is publicly available as of the date of publication. DOIs are listed in the key resources table.
- Any additional information required to reanalyze the data reported in this paper is available from the lead contact upon request.

EXPERIMENTAL MODEL AND SUBJECT DETAILS

The laboratory population of *H. miamia* adults represent many generations derived from 120 sexually reproducing worms collected from Bermuda in 2010[14,15]. The embryos used in this study were the progeny of random matings of these worms, Adult *Hofstenia* were cultured at 21°C in plastic boxes containing 1 Liter of filtered artificial sea water with 37 parts per thousand Instant Ocean sea salt (AFSW). Twice a week, boxes were cleaned, AFSW

renewed, and animals were fed freshly-hatched artemia. Embryos were laid spontaneously, in clutches, on the plastic substrate.

METHOD DETAILS

Generation and maintenance of transgenic lines—We generated a stable transgenic line that expresses the photoconvertible protein Kaede under the control of an *alpha-tubulin* (*tuba*) promoter. Identification and cloning of regulatory elements, mRNA injection, and transgenic animal care were done using the protocols developed in Ricci and Srivastava[23]. The transcript sequence of the *tuba* gene were identified in the *Hofstenia* transcriptome and the corresponding genomic locus was determined via BLAST. Primers were designed to amplify regions located 5' to the ATG and 3' to the STOP codon from genomic DNA (Genbank Genome accession SCFE00000000, *tuba* promoter genomic coordinate scaffold1:46,289,791-46,291,668, and *tuba* 3'UTR coordinate scaffold1:46,293,025-46,293,590). A cassette with Kaede-encoding sequence flanked by the *tuba* promoter and 3' UTR and SceI meganuclease sites was cloned into the backbone vector. Following cloning, plasmid isolation and sequencing were performed to assess proper fragment insertion.

Prior to injection, 4 μg of the desired plasmid was fully digested with 4 μl of I-SceI enzyme (Cat#R0694S), in a 50 μl reaction with 1X Outsmart buffer (Cat#B7204), left 1 to 2 hrs at 37 °C, followed by 20 minutes of heat inactivation at 65 °C. The digested plasmid was loaded in a 0.8% agarose SeaKem® GTG™ (Cat#50070, Lonza) gel. The fragment corresponding to the transgenic cassette was cut from the gel, purified with the NucleoSpin® Gel and PCR Clean-Up kit (Cat#740609, Macherey-Nagel), eluted in 15-30 μl of elution buffer and quantified with a NanodropND-1000 spectrophotometer. The injection solution was prepared in a volume of 10 μl, by assembling the following reagents in nuclease-free water, in order to obtain the given final concentration: digested DNA (10-25 ng/μl); Fluorescein Dextran (D1820, Invitrogen; 1.25 μg/μl); 1X I-SceI Buffer; I-SceI enzyme (Cat#R0694S, NEB; 0.375 U/μl).

To inject embryos, injection dishes were prepared, where an injection mold (composed of 300μm x 300μm square pins) was pressed into molten agarose in a 60x15mm culture dish. Individual embryos were pressed into the 300μm x 300μm holes created by the mold to keep in place during the injection process. A quartz needle (Cat#QF100-70-10, Sutter Instrument) was back-loaded with 0.75 μl of the injection solution and manipulated with Narishige MMN1 and MO202U micro-manipulators. Injections were performed under a Leica MZ10F Stereomicroscope, using a Pico-liter Microinjector (Cat# PLI-90A, Warner Instruments). After injection, embryos were placed in artificial seawater (ASW) with penicillin and streptavidin antibiotics (Cat#15140122, Thermofisher Scientific) at 5U/ml and left to grow in a 23°C incubator. The embryos were placed in normal ASW only after 5 days.

Based on data from the Hatchling Juvenile single cell RNAseq dataset, *tuba* mRNA in *Hofstenia* is expressed highly among the neoblasts of hatched juvenile worms[16]. However, in the transgenic embryos, Kaede protein fluorescence was detected in high amounts in the germline and oocytes, resulting in embryos and hatchling juvenile worms that showed ubiquitous fluorescence. This allowed for the fate-mapping experiments to take place.

Photoconversion and imaging for fate mapping—To photoconvert early embryonic cells, we first mounted embryos on a glass slide in artificial seawater (ASW), and lightly compressed them with a glass coverslip with “clay-feet”. We then rolled the embryos underneath the coverslip to orient the blastomere of interest towards the objective. Once embryos were properly mounted, we used a Leica SP8 confocal microscope under the 63x oil objective to photoconvert the blastomere of interest. We found that a laser power of 70% under the 405nm laser was sufficient to photoconvert the blastomeres after a 3-4 seconds of exposure. The length of time spent photoconverting was variable depending on the amount of Kaede fluorescence a particular individual had. After photoconversion, embryos were recovered from their slide by carefully peeling back the coverslip and using a glass pipette. All kaede transgenic embryos were protected from ambient light at all times, as we found that even low levels of ambient light could trigger some levels of photoconversion in the worm. To image photoconverted embryos, we mounted them in between a glass slide and a coverslip with “clay-feet” in ASW. Imaging of embryos was done with the Leica SP8 confocal microscope under the 20x objective. For experiments where tissue contributions of blastomeres were observed, we imaged worms immediately after hatching. To image photoconverted hatchlings, we compressed the animals until they were no longer able to move. To do this, we mounted them in between a glass slide and a coverslip in ASW. We used very minimal amounts of clay for the clay-feet to ensure sufficient compression of the animal. A “whole body” image was taken under the 10x objective, and higher magnification imaging which showcased the different labeled cell types was done using the 63x oil objective. Hatched worms were all imaged live.

Irradiation—Irradiation experiments were performed using a Radiation International, INC. Model B34 machine. All animals were placed in 60 x 15mm culture dishes in ASW and irradiated (10,000 rads) for 30 minutes. Animals were allowed to recover in normal ASW in a 23°C incubator, and were imaged after 7 days.

Regeneration assays—To perform regeneration assays, we placed recently hatched animals into a 70mm petri dish lined with Whatman filter paper. The animals were then cut in half along the transverse plane using a razor blade (Fine Science Tools Item no. 10316-14) and a Leica MZ10F stereomicroscope. The resulting head and tail pieces were then kept in separate wells in a 24-well plate to prevent the head pieces from cannibalizing the tails. Note that the worms were not fed at any point of this experiment. Fragments were then imaged 4 days after cutting. Embryos were cut in half using the same method described above, but were first treated in a previously outlined embryo de-shelling solution (composed of 32mM sodium hydroxide, 0.5mg/ml of sodium thioglycolate, and 1mg/ml of pronase in ASW)[15]. The egg shells were subsequently removed by shearing the embryos against a sharp, glass pipette.

Blastomere ablation experiments—Early embryo blastomeres were ablated using an IR laser at 1.45μm wavelength (XYClone, Hamilton Thorne Biosciences) that was mounted on a Leica DM5000 compound microscope. Embryos were placed in calcium and magnesium free ASW, and multiple laser pulses at 85% power were applied to the outer edges of blastomeres to be ablated. These pulses were applied in quick succession

to different parts of the outer edge of the blastomere, as single pulses resulted in the cell rupture briefly, but close back up again. The quick succession of multiple pulses should result in the majority of the inner cytoplasmic contents to spill out. After ablation, embryos were allowed to recover and develop in 60x55mm culture dishes in fresh ASW at 23°C.

RNAi knockdown experiments—In vitro double-stranded RNA preparation and injection of hatchling worms were done using established protocols[14]. dsRNA injections were performed using a Drummond Nanoject II. Animals were injected and soaked with dsRNA for 3 days, and then amputated. The fragments were then injected and soaked with dsRNA for 3 days, and then amputated again. We found a phenotype associated with the original tail fragment from which anterior tissue had been removed twice, as depicted in Figure S5K and S5L.

H3P staining—Phosphorylated Histone H3 (H3P) staining was performed using the methods previously published[14]. Embryos were placed in deshelling solution (composed of 32mM sodium hydroxide, 0.5mg/ml of sodium thioglycolate, and 1mg/ml of pronase in ASW) on a nutator. The incubation time differed depending on the developmental stage. Early cleavage to Pill stages were incubated for 8mins, whereas Prehatchling and Pigmented Prehatchling stages were incubated for 6mins. Embryos were then fixed in 4% Paraformaldehyde in ASW at 4°C overnight. Embryos were stored in 4°C in PBS for a maximum of one week before being used for H3P staining. H3P antibodies (Santa Cruz Biotechnology, Cat#sc-374669) were diluted 1:1000 in phosphate buffer solution (PBS), and samples were incubated in this solution for 1 hour at room temperature. The H3P antibodies were then washed out using four, 20min incubations in PBS.

Cell dissociation and FACS—Cell dissociation was done using previously published protocols[23]. Animals were placed in calcium and magnesium free ASW with 1% horse serum, and were vigorously pipetted up and down until they dissociated into single cells. After dissociation, the cell suspension was passed through a 40μm strainer into a 2mL tube. Excess debris was then eliminated by centrifuging the cells for 5mins at 500g (4°C) through a 4% BSA solution in calcium magnesium free ASW. All cell debris was expected to be caught at the interface of the 4% BSA solution and the cell suspension. The cell pellet was then resuspended in calcium magnesium free ASW with 1% horse serum. The resuspended cell suspension was then stained with Calcein Blue AM (Thermofisher C1429) to stain live cells. The Calcein Blue AM signal was used to sort for live cells. For our experiments, we dissociated 18 freshly hatched photoconverted worms to determine the transcriptional profile of 3a/3b progeny upon hatching, and 20 photoconverted embryos at 80 hours post laying to determine the transcriptional profile of 3a/3b progeny during embryogenesis. FACS was done using a Beckman Coulter MoFlo Astrios EQ Cell Sorter at the Harvard Bauer Core facility. Cells were sorted based on red vs green fluorescence among those that were positive for calcein (Fig. S4A and S5E). Cells were directly sorted into 96-well plates filled with a lysis buffer, with a total of 288 cells captured for sequencing for the hatchlings, and 96 cells captured for sequencing for the 80hpl embryos.

SMARTseq and SeqWell data collection and single cell analysis—Upon performing FACS, sequencing libraries were prepared by the Harvard Bauer Core facility using the SMARTseq2 protocol[38] for the photoconverted hatchling dataset, and the seqWell plexwell library prep (seqWell, sku:pw096) for the photoconverted embryo dataset (Post Dimple 80 hpl). Sequencing was also done by the Harvard Bauer Core facility using the Illumina Novaseq (100bp, paired end). Reads were demultiplexed, and then quantified using Salmon[39]. The resulting counts were then merged into a single table using a series of custom python scripts that are available on github: https://github.com/JulianKimura/SMARTseq_Pipeline. Once the merged count file was created, it was then imported into Seurat for downstream analysis. All of the code for clustering, plot generation, and statistical tests will be available on github. Cell type identities were assigned to the clusters by projecting marker genes for cell clusters identified in the Hatchling Juvenile dataset[16]. Specific genes were selected based on their specificity to their respective clusters in the Hatchling Juvenile dataset, and were compiled into a list of diagnostic genes (Table S1 and S2). Justifications for gene names are in Table S3. All raw fastq files for the sequencing data will be deposited into the NCBI sequence read archive (SRA).

Fluorescent in situ hybridization—mRNA localization was visualized using fluorescent *in situ* hybridization (FISH) described previously[15]. Embryos were placed in deshelling solution (composed of 32mM sodium hydroxide, 0.5mg/ml of sodium thioglycolate, and 1mg/ml of pronase in ASW) on a nutator. The incubation time differed depending on the developmental stage. Early cleavage to Pill stages were incubated for 8mins, whereas Prehatchling and Pigmented Prehatchling stages were incubated for 6mins. Embryos were then fixed in 4% Paraformaldehyde in ASW at 4°C overnight. Embryos were stored in 4°C in PBS for a maximum of one week before use in *in situ* hybridization. Embryos were washed out of PBS, and treated with proteinase K for 1 min (Early Cleavage to Pill stage embryos) and 3mins (Prehatchling to Hatched Juveniles). After treatment with proteinase K, embryos were placed in a 8M urea based pre-hybridization and hybridization solution.[15] Prehybridization took place for 2 hours, while hybridization took place overnight. After hybridization, samples were taken through a series of wash steps. Two 20min incubations in Prehybridization solution, two 20min incubation in a 50:50 mixture of Prehybridization solution and 2x saline sodium citrate buffer with (SSCT), two 20min incubations in 2x SSCT, and two 20min incubations in 0.2x SSCT. Samples were then placed in either anti-Digoxigenin-POD (1:1500 dilution) or anti-Fluorescein (1:2000 dilution) in blocking solution at 4°C overnight. Samples were then washed ten times for 20mins each in PBST, and were then incubated with Tyramide with rhodamine of Fluorescein (1:1000 and 1:2000 respectively) with hydrogen peroxide (0.002% final concentration) for 10mins on a nutator. Samples were then washed with PBST, and imaged with a Leica SP8 confocal microscope.

Cell dissociation and InDrops encapsulation and library preparation—Embryos at various developmental stages (35, 50, 65, 80, 95, 110, 125, and 145 hours post laying) were placed in a de-shelling solution for various lengths of time using the recipe detailed both above and in a previous publication (See Fluorescent in situ Hybridization)[15]. Once the embryos were de-shelled, embryos were dissociated and prepped for in drops encapsulation

using the methods described above and in a previous study[16]. Single cell suspensions were encapsulated using the in drops platform at the Harvard University Single Cell Core[24]. *Hofstenia* is a marine organism, meaning that their cells needed to be in artificial seawater to maintain osmoregularity as long as possible before being encapsulated. To allow for this, we utilized a specialized microfluidics chip that had a separate channel that supplied phosphate buffer solution (PBS) just prior to the cells being encapsulated[16]. The subsequent library preparation was done by the Harvard Single Cell Core, following the standard indrops protocol where transcripts are barcoded within individual droplets in oil[24]. The qPCR quantification and sequencing of libraries was done using the KAPA Library Quantification Kit (Roche, material# 7960140001) and the illumina Nextseq sequencer (75bp, paired end).

Analysis of InDrops single cell data and trajectory inference—Demultiplexing, mapping, quantification, and generation of count matrices were done using the protocols described in the github repository: https://github.com/brianjohnhaas/indrops. All read and count numbers are in Table S1D. The subsequent downstream analysis of clustering was performed using the R package Seurat[40–43]. Doublets and low quality cells were filtered based on outliers in the number of genes expressed per cell, and the number of UMIs detected. Trajectory inference and differential expression of molecular trajectories of the embryonic data were done using the R package URD[26]. URD does not allow for datasets above 45,000 cells. Thus, we randomly subsampled our original 51,000 cell dataset into 43,000 cells. The root for the URD tree was defined as cells from the Gastrula stage (35hpl), and the tips for the tree were defined as the cell clusters identified in the *Hofstenia* Hatchling Juvenile[16].

QUANTIFICATION AND STATISTICAL ANALYSIS

Single cell RNA-seq—All differential expression analysis for calling marker genes for clusters was done using the default method in the Seurat package (Wilcoxon rank sum test). A Chi squared test of independence was done using the base R command to test the significance of cell types and their identities (Red vs Green). A Wilcoxon ranked sum test was performed to determine the significance of the expression levels of *piwi-1* between the red and green cells. All differential expression for trajectory inference were done using the default area under precision recall (AUPRC) test, as detailed in a previous publication[26].

Supplementary Material

Refer to Web version on PubMed Central for supplementary material.

Acknowledgements

We thank Elizabeth D'Haiti for help in generating data showing the distribution of H3P during embryogenesis, and Dr. Yi-Jyun Luo for help in generating the count matrices for the InDrops single cell RNA-seq dataset. We also thank the Harvard Bauer Core Facility for assistance with FACS and with generating, sequencing, and demultiplexing SMARTseq libraries. We also thank members of the Srivastava Lab for intellectual discussions, feedback on the manuscript, and other support in the laboratory. L.R. and M.S. were supported by grants to M.S. by the Searle Scholars Program (SSP-2016-1494), Smith Family Foundation, and the National Institutes of Health (1R35GM128817). D.M.B.R. was supported by National Institutes of Health (1R35GM128817). J.O.K. was supported by the Department of Organismic and Evolutionary Biology, the NSF-Simons Center for Mathematical and Statistical Analysis of Biology at Harvard, and the Harvard Quantitative Biology Initiative (1764269).

References Cited

1. Lai AG and Aboobaker AA (2018). EvoRegen in animals: Time to uncover deep conservation or convergence of adult stem cell evolution and regenerative processes. Dev. Biol 433, 118–131. [PubMed: 29198565]
2. Randolph H (1897). Observations and Experiments on Regeneration in Planarians.
3. Wagner DE, Wang IE and Reddien PW (2011). Clonogenic neoblasts are pluripotent adult stem cells that underlie planarian regeneration. Science 332, 811–816 (2011). [PubMed: 21566185]
4. Buchanan JW (1933) Regeneration in Phagocata gracilis (Leidy). Physiol. Zool 6, 185–204.
5. Müller WA, Teo R and Frank U (2004). Totipotent migratory stem cells in a hydroid. Dev. Biol 275, 215–224. [PubMed: 15464584]
6. Gahan JM, Bradshaw B, Flici H and Frank U (2016). The interstitial stem cells in Hydractinia and their role in regeneration. Curr. Opin. Genet. Dev 40, 65–73. [PubMed: 27379898]
7. Funayama N (2013). The stem cell system in demosponges: suggested involvement of two types of cells: archeocytes (active stem cells) and choanocytes (food-entrapping flagellated cells). Dev. Genes Evol 223, 23–38. [PubMed: 23053625]
8. De Sutter D and Van de Vyver G (1979). Isolation and recognition properties of some definite sponge cell types. Dev. Comp. Immunol 3, 389–397. [PubMed: 510654]
9. van Wolfswinkel JC (2014). Piwi and potency: PIWI proteins in animal stem cells and regeneration. Integr. Comp. Biol 54, 700–713. [PubMed: 24948137]
10. Yeo J-C and Ng H-H (2013). The transcriptional regulation of pluripotency. Cell Res. 23, 20–32. [PubMed: 23229513]
11. Davies EL, Lei K, Seidel CW, Kroesen AE, McKinney SA, Guo L, Robb SM, Ross EJ, Gotting K, and Alvarado AS (2017). Embryonic origin of adult stem cells required for tissue homeostasis and regeneration. Elife 6.
12. Rebscher N, Volk C, Teo R, and Plickert G (2008). The germ plasm component Vasa allows tracing of the interstitial stem cells in the cnidarian Hydractinia echinata. Dev. Dyn 237, 1736–1745. [PubMed: 18489004]
13. Leclère L, Jager M, Barreau C, Chang P, Le Guyader H, Manuel M, and Houliston E (2012). Maternally localized germ plasm mRNAs and germ cell/stem cell formation in the cnidarian Clytia. Dev. Biol 364, 236–248. [PubMed: 22309706]
14. Srivastava M, Mazza-Curll KL, van Wolfswinkel JC, and Reddien PW (2014) Whole-body acoel regeneration is controlled by Wnt and Bmp-Admp signaling. Curr. Biol 24, 1107–1113. [PubMed: 24768051]
15. Kimura JO, Ricci L, and Srivastava M (2021). Embryonic development in the acoel Hofstenia miamia. Development 148.
16. Hulett RE, Kimura JO, Marcela Bolanos D, Luo Y-J, Ricci L, and Srivastava M (2022). Acoel single-cell atlas reveals expression dynamics and heterogeneity of a pluripotent stem cell population. bioRxiv 2022.02.10.479464.
17. Fincher CT, Wurtzel O, de Hoog T, Kravarik KM, and Reddien PW (2018). Cell type transcriptome atlas for the planarian Schmidtea mediterranea. Science.
18. van Wolfswinkel JC, Wagner DE, and Reddien PW (2014). Single-cell analysis reveals functionally distinct classes within the planarian stem cell compartment. Cell Stem Cell 15, 326–339. [PubMed: 25017721]
19. Scimone ML, Kravarik KM, Lapan SW, and Reddien PW (2014). Neoblast specialization in regeneration of the planarian Schmidtea mediterranea. Stem Cell Reports 3, 339–352. [PubMed: 25254346]
20. Martindale MQ & Hejnol AA (2009). developmental perspective: changes in the position of the blastopore during bilaterian evolution. Dev. Cell 17, 162–174. [PubMed: 19686678]
21. Martindale MQ, Pang K & Finnerty JR (2004). Investigating the origins of triploblasty: ‘mesodermal’ gene expression in a diploblastic animal, the sea anemone Nematostella vectensis(phylum, Cnidaria; class, Anthozoa). Development 131 2463–2474. [PubMed: 15128674]

22. Meyer NP, Boyle MJ, Martindale MQ, and Seaver EC (2010). A comprehensive fate map by intracellular injection of identified blastomeres in the marine polychaete Capitella teleta. EvoDevo 1.
23. Ricci L and Srivastava M (2021) Transgenesis in the acoel worm Hofstenia miamia. Dev. Cell 56, 3160–3170.e4. [PubMed: 34752780]
24. Zilionis R, Nainys J, Veres A, Savova V, Zemmour D, Klein AM, and Mazutis L (2017). Single-cell barcoding and sequencing using droplet microfluidics. Nat. Protoc 12, 44–73. [PubMed: 27929523]
25. McInnes L, Healy J, Saul N and Großberger L (2018). UMAP: Uniform Manifold Approximation and Projection. Journal of Open Source Software 3, 861.
26. Farrell JA, Wang Y, Riesenfeld SJ, Shekhar K, Regev A, and Schier AF (2018). Single-cell reconstruction of developmental trajectories during zebrafish embryogenesis. Science 360.
27. Henry JQ, Martindale MQ and Boyer BC (2000). The unique developmental program of the acoel flatworm, Neochildia fusca. Dev. Biol 220, 285–295. [PubMed: 10753516]
28. Raz AA, Wurtzel O and Reddien PW (2021). Planarian stem cells specify fate yet retain potency during the cell cycle. Cell Stem Cell 28, 1307–1322.e5. [PubMed: 33882291]
29. Extavour CG and Akam M (2003). Mechanisms of germ cell specification across the metazoans: epigenesis and preformation. Development 130, 5869–5884. [PubMed: 14597570]
30. Özpolat BD, Duygu Özpolat B, Handberg-Thorsager M, Vervoort M and Balavoine G (2017). Cell lineage and cell cycling analyses of the 4d micromere using live imaging in the marine annelid Platynereis dumerilii. eLife 6.
31. Kobayashi T and Kageyama R (2010) The cyclic gene Hes1 contributes to diverse differentiation responses of mouse embryonic stem (ES) cells by regulating Notch signaling activation. Neuroscience Research 68, e134.
32. Zhang X, Yalcin S, Lee D-F, Yeh T-YJ, Lee S-M, Su J, Mungamuri SK, Rimmelé P, Kennedy M, Sellers R, et al. (2011). FOXO1 is an essential regulator of pluripotency in human embryonic stem cells. Nat. Cell Biol 13, 1092–1099. [PubMed: 21804543]
33. Russell R, Ilg M, Lin Q, Wu G, Lechel A, Bergmann W, Eiseler T, Linta L, Kumar P P, Klingenstein M, et al. (2015). A Dynamic Role of TBX3 in the Pluripotency Circuitry. Stem Cell Reports 5, 1155–1170. [PubMed: 26651606]
34. Boehm A-M, Khalturin K, Anton-Erxleben F, Hemmrich G, Klostermeier UC, Lopez-Quintero JA, Oberg H-H, Puchert M, Rosenstiel P, Wittlieb J, et al. (2012). FoxO is a critical regulator of stem cell maintenance in immortal Hydra. Proc. Natl. Acad. Sci. U. S. A 109, 19697–19702. [PubMed: 23150562]
35. Cannon JT, Vellutini BC, Smith J 3rd, et al. (2016) Xenacoelomorpha is the sister group to Nephrozoa. Nature 530(7588): 89–93. [PubMed: 26842059]
36. Kapli P and Telford MJ (2020). Topology-dependent asymmetry in systematic errors affects phylogenetic placement of Ctenophora and Xenacoelomorpha. Science advances 6(50). DOI: 10.1126/sciadv.abc5162.
37. Philippe H, Poustka AJ, Chiodin M, et al. (2019) Mitigating Anticipated Effects of Systematic Errors Supports Sister-Group Relationship between Xenacoelomorpha and Ambulacraria. Current biology: CB 29(11): 1818–1826.e6. [PubMed: 31104936]
38. Picelli S, Björklund ÅK, Faridani OR, Sagasser S, Winberg G, and Sandberg R (2013). Smart-seq2 for sensitive full-length transcriptome profiling in single cells. Nat. Methods 10, 1096–1098. [PubMed: 24056875]
39. Patro R, Duggal G, Love MI, Irizarry RA and Kingsford C (2017). Salmon provides fast and bias-aware quantification of transcript expression. Nat. Methods 14, 417–419. [PubMed: 28263959]
40. Butler A, Hoffman P, Smibert P, Papalexi E and Satija R (2018). Integrating single-cell transcriptomic data across different conditions, technologies, and species. Nat. Biotechnol 36, 411–420. [PubMed: 29608179]
41. Hao Y, Hao S, Andersen-Nissen E, Mauck WM 3rd, Zheng S, Butler A, Lee MJ, Wilk AJ, Darby C, Zager M, et al. (2021). Integrated analysis of multimodal single-cell data. Cell 184, 3573–3587.e29. [PubMed: 34062119]

42. Satija R, Farrell JA, Gennert D, Schier AF and Regev A (2015). Spatial reconstruction of single-cell gene expression data. Nat. Biotechnol 33, 495–502. [PubMed: 25867923]

43. Stuart T, Butler A, Hoffman P, Hafemeister C, Papalexi E, Mauck WM 3rd, Hao Y, Stoeckius M, Smibert P, and Satija R (2019). Comprehensive Integration of Single-Cell Data. Cell 177, 1888–1902.e21. [PubMed: 31178118]

HIGHLIGHTS

- Photoconversion-based lineage tracing reveals fate map for *H. miamia* embryos
- Two micromeres at the 16-cell stage are the likely embryonic source of stem cells
- Single-cell developmental atlas provides molecular trajectories for stem cells
- Labeling and isolation of stem cell lineage corroborates molecular components

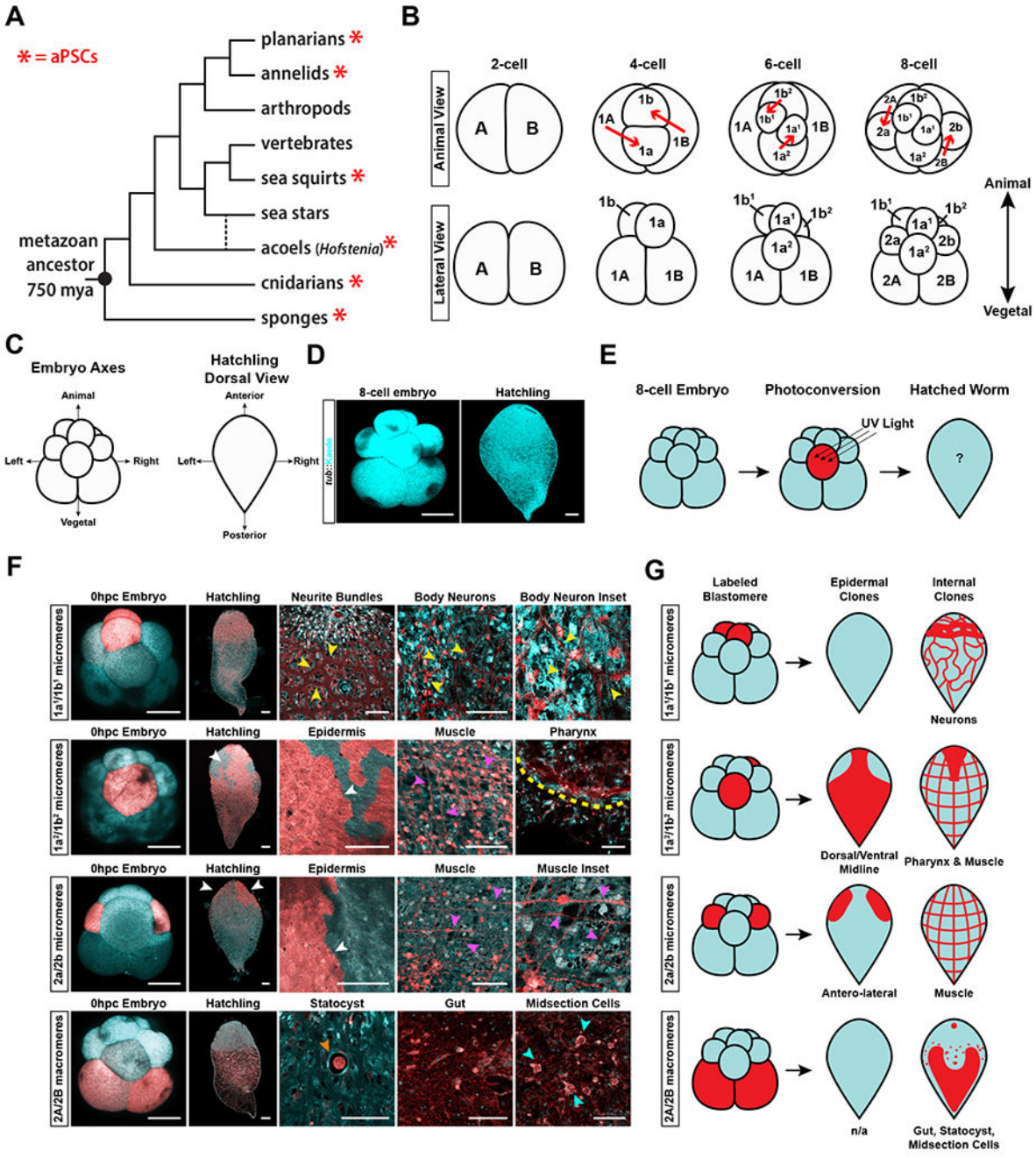

Figure 1: Lineage tracing using photoconvertible transgenic embryos reveals the cellular sources for major tissue types.

(A) Metazoan tree of life showing the widespread occurrence of adult pluripotent stem cells (aPSCs) (red asterisk) in many lineages and their absence in mammals (vertebrates). The branch for acoels is dotted to indicate two phylogenetic positions currently under debate[35–37]. (B) Schematic diagram showing the stereotyped duet cleavage pattern of *Hofstenia miamia* embryos from the 2-cell to 8-cell stage. Top: Animal view of the cleavage pattern. Red arrows show the direction of cleavage to generate blastomeres. Bottom: Lateral view of embryos. The animal and vegetal axis corresponding to the lateral view is denoted

in bold arrows (C) Schematic diagram of embryonic and adult axes, relating to D, E, F, and G. Left: Embryonic axes labeled at the 8-cell stage embryo when viewed laterally. Right: Adult body axes labeled on a hatchling worm when viewed from the dorsal side. (D) Images of a *tuba*::Kaede transgenic 8-cell stage embryo and hatchling worm (pseudo-colored in cyan). (E) Schematic showing the workflow for photoconversion. (F) Fate-mapping of 8-cell state embryos via photoconversion of pairs of blastomeres. Single-cell conversions are shown in Fig. S1D. $1a^1/1b^1$ cells give rise to neurons in the adult, with large neurite bundles being visible in the anterior, and a net-like structure of body neurons throughout the body (yellow arrowheads) (n=10/10). $1a^2/1b^2$ cells give rise to the dorsal-ventral-midline epidermis (white arrowhead), muscle (magenta arrowheads), and the pharynx (yellow dotted line) (n=12/12). 2a/2b cells give rise to the anterior-lateral epidermis (white arrowheads), and muscle (magenta arrowheads) (n=6/6). 2A/2B cells give rise to the statocyst (orange arrowhead), gut, and a population of internal, midsection cells (cyan arrowheads) (n=4/4). The same worms shown here were also followed during embryonic development, shown in Fig. S1C. (G) Schematic diagrams of the cell types generated by each pair of blastomeres. All images of hatchlings were taken with a 10x objective, all embryo images were taken under 20x magnification. Images of specific tissues, regions, or insets were taken at high magnification under a 63x objective. Embryo and hatchling scale bars = 100μm. High magnification image scale bars = 50μm. See also Figure S1, Video S1, Video S2, Video S3, and Videol S4.

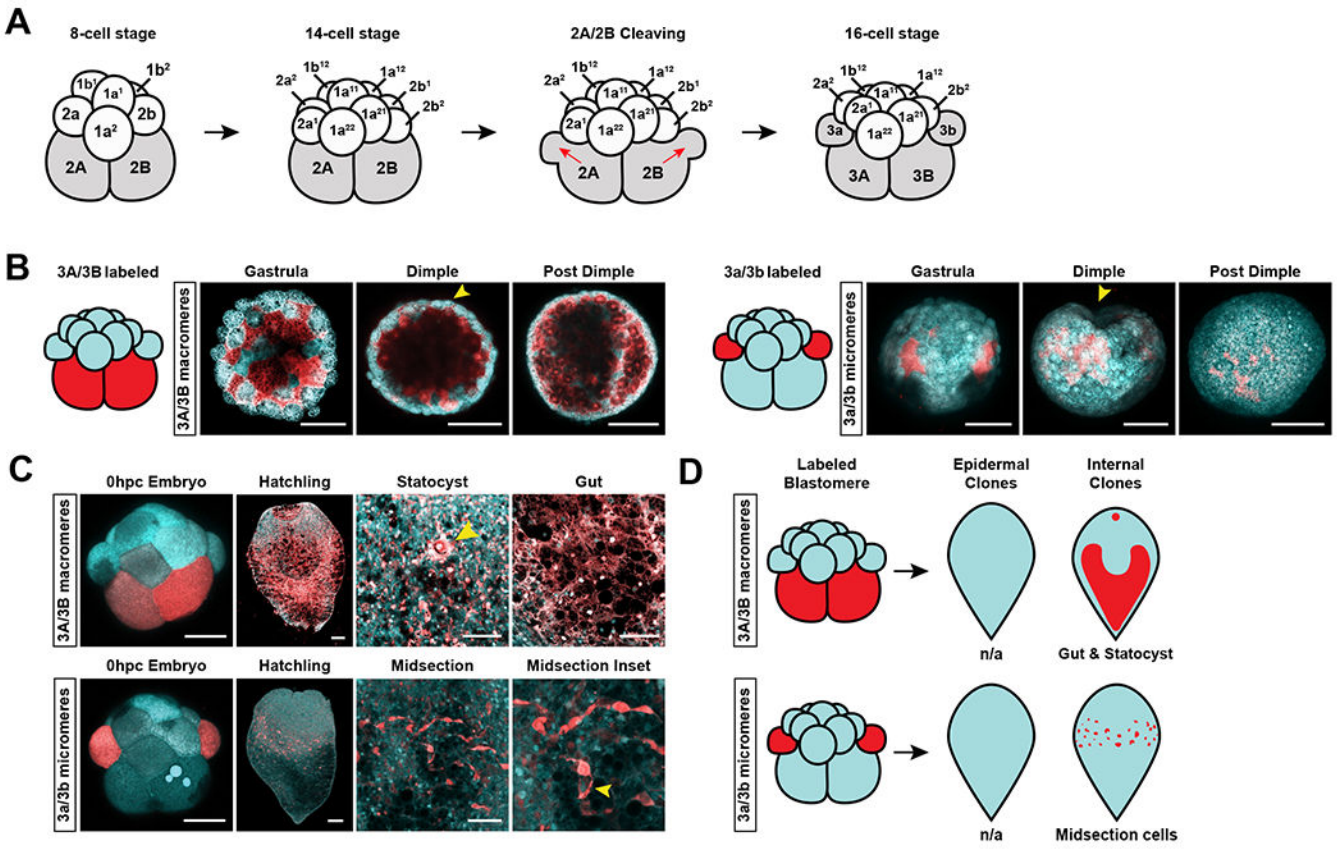

Figure 2: Progeny of 3a/3b, but not of 3A/3B, are midsection cells that resemble neoblasts in spatial distribution.

(A) Lateral view schematic of an 8-cell stage embryo cleaving to form the 16-cell stage embryo. 2A/2B blastomeres cleave to form micromeres 3a/3b and macromeres 3A/3B. Red arrows show the direction of cell division. (B) Tracing the fates of 3A/3B and 3a/3b progeny during embryonic development. Yellow arrow heads denote the site of the ”dimple”. Left: Embryonic time series of 3A/3B progeny after photoconversion. All progeny were internalized at the Gastrula stage. Right: Embryonic time series of 3a/3b progeny after photoconversion. Progeny occupied two external patches at the Gastrula stage that were subsequently internalized at the Dimple stage adjacent to the site of the “dimple” (yellow arrowhead) (C) Top row: 3A/3B progeny form the gut and statocyst (yellow arrowhead). Bottom row: 3a/3b cell progeny form a population of midsection cells that were seen amongst the 2A/2B progenies. Midsection inset shows cytoplasmic extensions of the cells (yellow arrowhead). (D) Schematic diagram of the distribution of 3A/3B and 3a/3b progeny in the hatched worm. Embryo and hatchling scale bars = 100μm. High magnification image scale bars = 50μm. See also Figure S2 and Video S4.

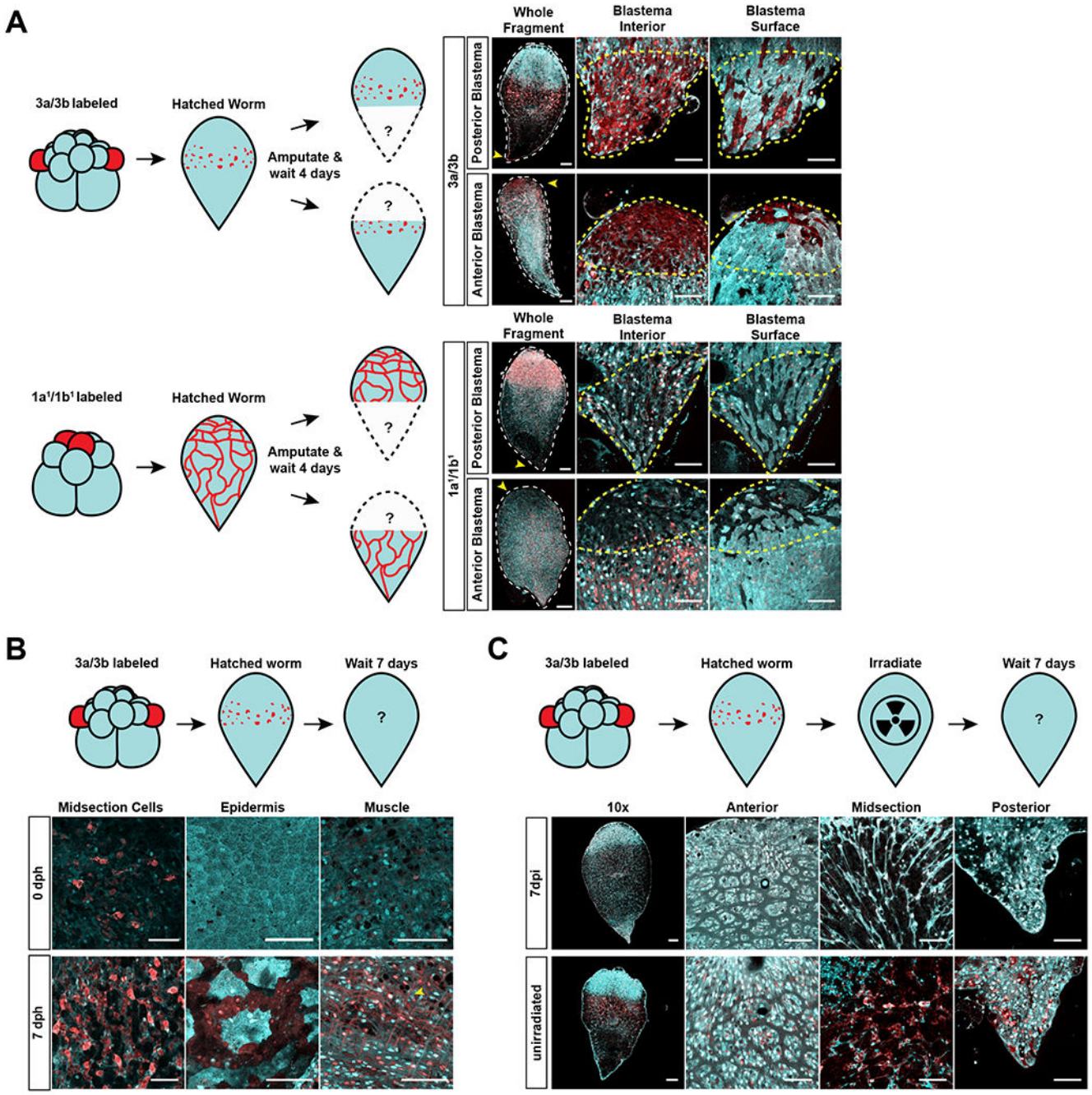

Figure 3: 3a/3b micromere progeny exhibit functional characteristics of neoblasts.

(A) Top Left: Schematic of experimental design for testing the contribution of 3a/3b progeny to the blastema. Top Right: Red labeling from the 3a/3b progeny spread to the blastema (yellow arrowhead in whole fragment images, outlined in yellow dashed lines in high magnification images of blastema) during anterior (n=5/5) and posterior regeneration (n=3/3), showing contribution to newly regenerated tissue. Both interior and surface z-slices of the blastema show the spread of red labeling to new tissue. Bottom Left: Schematic of experimental design for testing the contribution of $1a^1/1b^1$ progeny to the blastema.

Bottom Right: Red labeling from the $1a^1/1b^1$ progeny did not spread to the blastema (yellow arrowhead in whole fragment images, outlined in yellow dashed lines in high magnification images of blastema) during anterior (n=3/3) or posterior regeneration (n=3/3), showing absence of contribution to newly regenerated tissue. Both interior and surface z-slices of the blastema do not show the spread of red labeling to new tissue. Images to the right of the hatchling images show high magnification views of relevant areas. Scale bars for hatchling images = 100μm. Scale bars for high magnification images = 50μm. Progeny of other blastomeres at the 16-cell stage also did not contribute to newly regenerated tissue– see Fig. S3B and S3C. (B) Top: Schematic of experimental design for testing the contribution of 3a/3b progeny to homeostatic tissue differentiation. Bottom: At 7 days post hatching (dph), 3a/3b labeled worms showed an increase in the number of midbody cells as well as presence of red labeling to epidermis and muscle (3/3), which were absent in animals that had just hatched (0 dph) (3/3). Scale bars = 50μm. Progeny of other blastomeres that normally do not contribute to epidermis or muscle showed no detectable contribution to these tissues during homeostasis – see Fig. S3D (C) Top: Schematic of experimental design for testing the sensitivity of 3a/3b progeny to radiation. Bottom: 3a/3b progeny are not detectable 7 days post irradiation (dpi) (4/4), in contrast to in unirradiated worms (3/3). Progeny of other blastomeres were not irradiation sensitive - see Fig. S3E. Images to the right of the hatchling images show high magnification views of relevant areas. Scale bars for hatchling images = 100μm. Scale bars for high magnification images = 50μm. See also Figure S3.

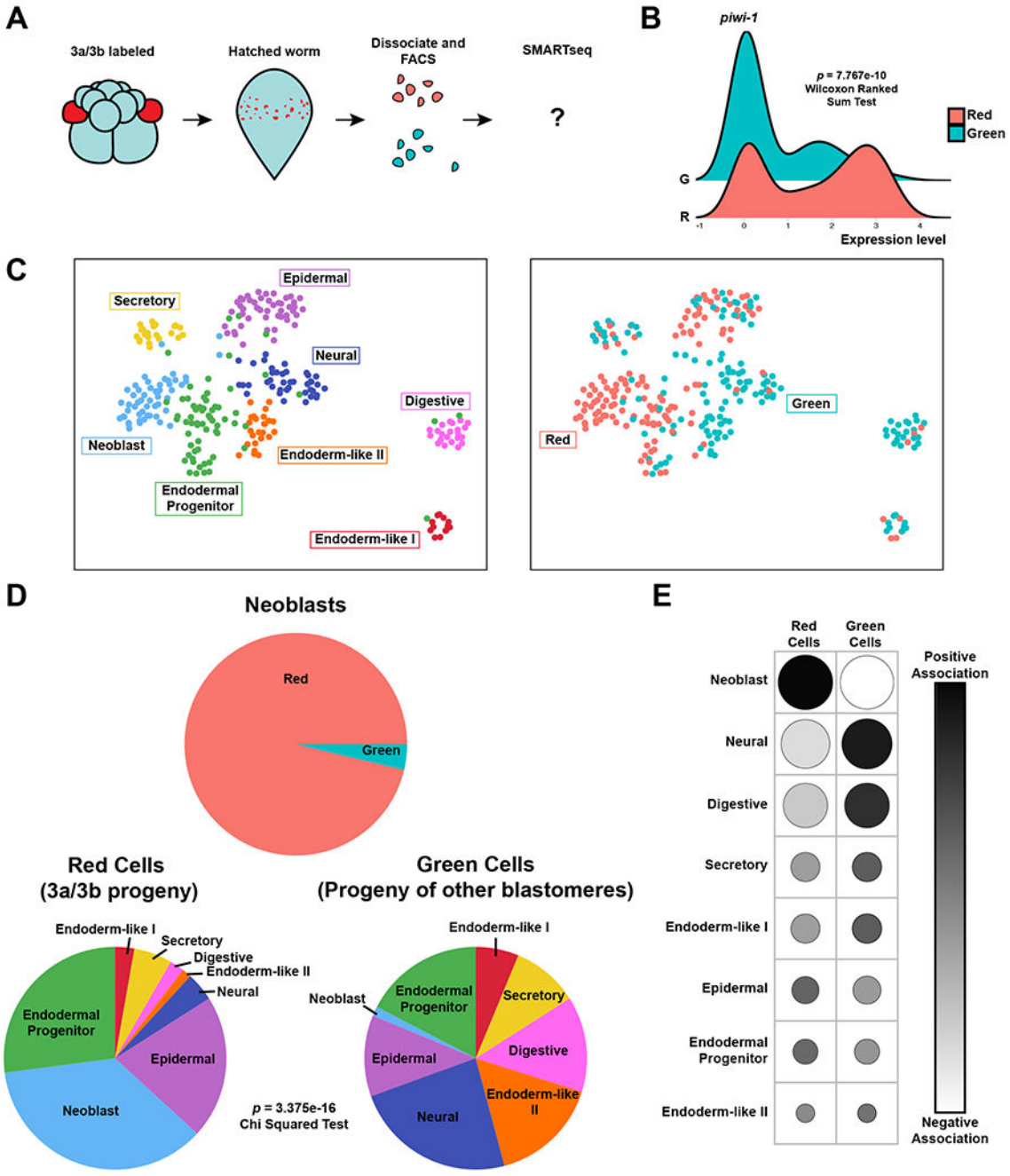

Figure 4: Single-cell profiling of 3a/3b micromere progeny shows they exhibit molecular characteristics of neoblasts.

(A) Schematic diagram of experimental design. Worms with labeled 3a/3b progeny were dissociated, and cells sorted based on red vs green (shown in cyan) fluorescence. A total of 288 sorted cells were then sequenced via SMARTseq. (B) Ridgeplot of the relative expression levels of the neoblast marker *piwi-1* between red and green cells (p-value = 7.767e-10, Wilcoxon Ranked Sum Test). (C) Left: UMAP of sequenced cells showing cluster identity, which corresponds to clearly identifiable cell types, including neoblasts. Right: Corresponding UMAP with colors showing the photoconversion status of red (3a/3b

progeny) and green cells (progeny of other blastomeres). The vast majority of the neoblast cluster is composed of red cells (3a/3b progeny). (D) Top: Pie chart showing the proportion of red (52/54) and green (2/54) cells in the neoblast cluster. Bottom: Pie charts showing the proportion of red (3a/3b progeny) and green (progeny of other blastomeres) cells that belong to different cell clusters. Red cells have a significantly larger proportion of neoblasts compared to green cells. Chi squared test of independence showed statistically significant association of cell types to their red vs green label color (p-value = 3.375e-16). (E) Contingency table showing the Pearson residuals for each cell type and their label color (red vs green). Darker shades show positive association, negative association. Larger dots represent a higher degree of association, while smaller dots represents a smaller degree. Overall, red cells (3a/3b progeny) are largely defined by the presence of neoblasts, whereas green cells (progeny of other cells) are largely defined by the absence of neoblasts and the presence of other cell types. See also Figure S4, Table S1, and Table S3.

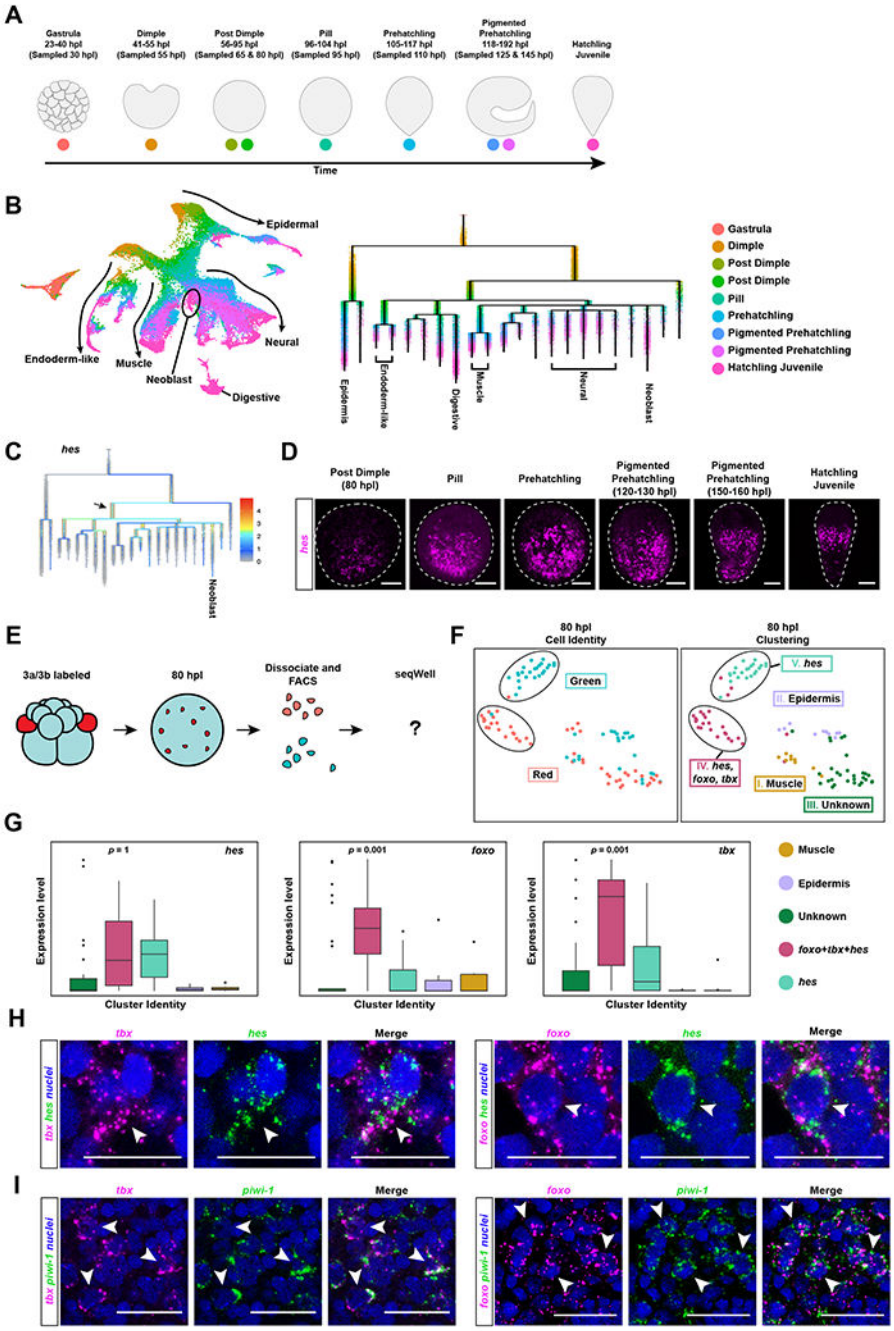

Figure 5: Combining embryo single-cell analysis and neoblast cell-lineage tracing reveals a molecular trajectory for neoblasts during development.

A) Schematic highlighting *Hofstenia* developmental stages and the developmental timing at which they were sampled to generate the single-cell RNA-seq dataset. (B) Left: UMAP plot of the embryonic dataset merged with the Hatchling Juvenile dataset[16] to obtain endpoints in development. Arrows and tissue-type labels highlight the UMAP topology, and the expression of known marker genes of the corresponding tissues as shown in Fig. S5A. Right: URD trajectory inference tree showing the putative molecular trajectories of cells in the form of a tree, with the branch tips annotated with known differentiated cell types[16].

Dots, representing cells, are colored based on developmental time points shown in A. (C) Expression levels of the gene *hes* projected onto the URD tree. We see high expression levels of *hes* at an internode that is populated largely by cells from the Post Dimple stage (80 hours post laying (hpl)) (black arrow) (D) *in situ* hybridization of *hes* reveals expression first detectable at the Post Dimple stage (80 hpl) which culminated in a neoblast-like pattern in hatchlings. (E) Schematic workflow for sorting and sequencing a total of 96 cells from Post Dimple stage (80 hpl) embryos with photoconverted 3a/3b progeny at single-cell resolution. Red cells represent 3a/3b progeny that should make neoblasts, whereas green cells are progeny of other blastomeres that give rise to differentiated cell types. (F) Left: UMAP showing photoconversion status (red, 3a/3b progeny; cyan, progeny of other, unconverted blastomeres). Right: UMAP showing cluster identities. Muscle (Cluster I; mustard) and epidermal (Cluster II; light purple) cells were detected. One cluster did not yield any markers with enriched expression, and is labeled as “Unknown” (Cluster III; dark green). Clusters that were predominantly composed of 3a/3b progeny (Cluster IV; cranberry) and predominantly composed unconverted progeny (Cluster V; light green) were detected (circled in black). Both of these clusters expressed *hes,* but the Cluster IV, composed of 3a/3b progeny, show significantly enriched expression of *foxo* and *tbx.* (G) Box plots showing *hes* was expressed in both of Cluster IV and Cluster V, corroborating the lineage analysis in B that *hes* marks undifferentiated embryonic progenitors for many cell types, *foxo I*and *tbx* were highly enriched in Cluster V, which consists primarily of 3a/3b progeny. Data represented as mean ± SEM. (H) Double *in situ* hybridization of *foxo* and *tbx* with *hes* in Pigmented Prehatchling (120 hpl) embryos shows co-localization (white arrowheads). (I) Double *in situ* hybridization of *foxo* and *tbx* with *piwi-1* in hatched worms shows co-localization (white arrowheads), confirming that both *foxo* and *tbx* mark a subset of neoblasts. Scale bars for embryo and hatchling images = 100μm. Scale bars for high magnification images = 50μm. See also Figure S5, Table S1, Table S2, and Table S3.

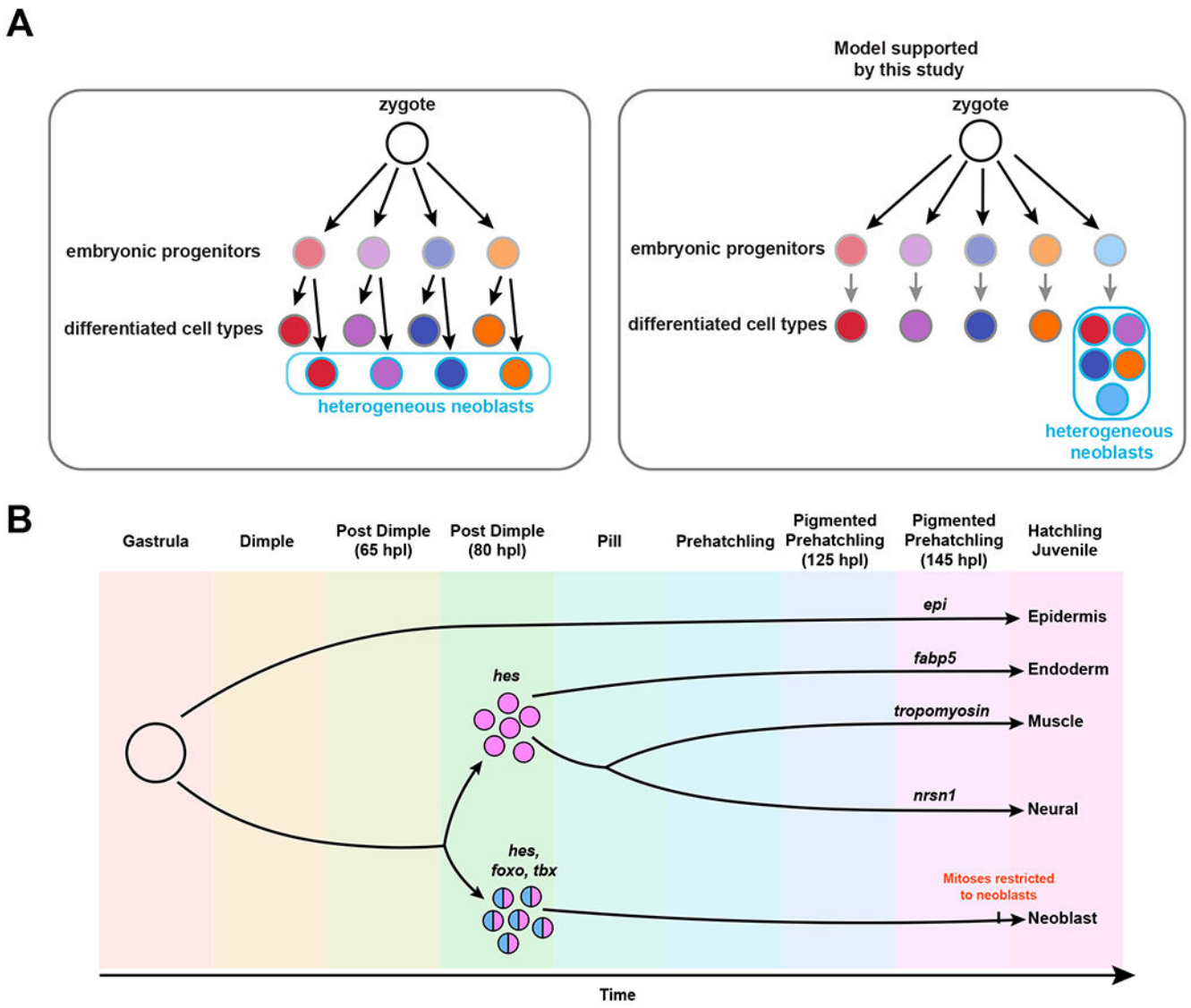

Figure 6: Models for the cellular and molecular origins of aPSCs.

(A) Schematics showing two hypotheses about the formation of heterogeneous aPSCs (neoblasts). Left: Scenario where distinct embryonic progenitors for differentiated tissues give rise to corresponding tissue-associated neoblast subtypes. Right: Model supported by our data, where the neoblast lineage becomes distinct from other cell lineages early in development, and become heterogeneous over time. Light grey outlines represent embryonic cells, dark gray outlines represent differentiated cell types in hatched worms, blue outlines represent neoblasts in hatched worms, fill colors correspond to different cell types: endoderm I (red), epidermis (purple), neural (dark blue), endoderm II (orange), neoblasts (light blue). B) Model depicting transcriptional lineages in development, highlighting *hes* as a marker of progenitors for multiple cell types, including neoblasts, and *foxo* and *tbx* as specific to the neoblast lineage. Although the neoblast lineage is distinct early in

development, functional neoblasts, as indicated by restriction of mitoses to *piwi-1*+ cells likely occurs late, close to hatching.

REAGENT or RESOURCE	SOURCE	IDENTIFIER
Antibodies		
Anti-H3P	Santa Cruz Biotechnology	Cat#sc-374669
Hofstenia specific Ab Anti-tropomyosin	GenScript	N/A (Available from the Lead Contact upon request)
Chemicals, peptides, and recombinant proteins		
Calcein AM	Invitrogen	Cat#65-0853-39
Instant Ocean sea salt	Instant Ocean	Cat#SS15-10
Agarose SeaKem® GTG™	Lonza	Cat#50070
TOPRO3	Thermofisher	Cat#T3605
Dextran, Fluorescein, 10,000 MW	Invitrogen	Cat#D1820
1X SceI Buffer	Benchmade	Cat#15140122
I-SceI enzyme	NEB	Cat#R0694S
Cutsmart Buffer	NEB	Cat#B7204
Critical commercial assays		
KAPA Library Quantification kit	Roche	Cat#7960140001
NucleoSpin® Gel and PCR Clean-Up kit	Macherey-Nagel	Cat#740609
Deposited data		
Gene Sequences	NCBI GenBank	hes (OP681623) foxo (OP681624) neo (OP681625) gland (OP681626) tbx (OP681627) grn (OP681628) epi (OP681629) s61a2 (OP681630) nrsn1 (OP681631) abcb6 (OP681632) nfic (OP681633) hexb (OP681634)
Sequencing Data	NCBI SRA	PRJNA889328 (FACS sorted 3a/3b progeny at hatching) PRJNA887118 (FACS sorted 3a/3b progeny at 80hpl) PRJNA888438 (Embryonic and Postembryonic datasets)
Experimental models: Organisms/ strains		
Hofstenia miamia	The animals used in this study are derived from random matings of the progeny of the original 120 worms collected in Bermuda in 2010.	N/A (Available from the Lead Contact upon request)
Recombinant DNA		
Plasmid *tubr::Kaede*	Generated for this paper; deposited to Addgene	Available from the Lead Contact upon request; Addgene plasmid ID: 193054
Software and algorithms		
Seurat	Hao et al. [41]	https://satijalab.org/seurat/
URD	Farrell et al.[26]	https://github.com/farrellja/URD
R	N/A	https://www.r-project.org/

REAGENT or RESOURCE	SOURCE	IDENTIFIER
All R scripts for single cell RNAseq analysis	This manuscript is the source of the R scripts for analysis	https://github.com/JulianKimura/Kimura_2022_Rscripts
Code used to generate SMARTseq matrices	This manuscript is the source of the code used to generate SMARTseq matrices	https://github.com/JulianKimura/SMARTseq_Pipeline
Other		
quartz needles	Sutter Instrument	Cat#QF100-70-10
Nunc™ bottom glass dishes	Thermo Scientific™	Cat#150682
Illumina Nextseq 500	Illumina	Cat#SY-415-1001
Illumina Novaseq 6000	Illumina	Cat#20012850
Moflo Astrios EQ	Beckman Coulter	Cat#B25982